

Nanoscale

Accepted Manuscript



This is an *Accepted Manuscript*, which has been through the Royal Society of Chemistry peer review process and has been accepted for publication.

Accepted Manuscripts are published online shortly after acceptance, before technical editing, formatting and proof reading. Using this free service, authors can make their results available to the community, in citable form, before we publish the edited article. We will replace this *Accepted Manuscript* with the edited and formatted *Advance Article* as soon as it is available.

You can find more information about *Accepted Manuscripts* in the [Information for Authors](#).

Please note that technical editing may introduce minor changes to the text and/or graphics, which may alter content. The journal's standard [Terms & Conditions](#) and the [Ethical guidelines](#) still apply. In no event shall the Royal Society of Chemistry be held responsible for any errors or omissions in this *Accepted Manuscript* or any consequences arising from the use of any information it contains.

Cite this: DOI: 10.1039/c0xx00000x

www.rsc.org/xxxxxx

FEATURE ARTICLE**Integrated optical antennas, and their impact on active optoelectronic devices****Alireza Bonakdar and Hooman Mohseni***Received (in XXX, XXX) Xth XXXXXXXXXX 20XX, Accepted Xth XXXXXXXXXX 20XX*

DOI: 10.1039/b000000x

Remarkable progress has been made in the fabrication and characterization of optical antennas that are integrated with optoelectronic devices. We describe the fundamental reasons for, and experimental evidence of the dramatic improvements that can be achieved by enhancing the light-matter interaction via an optical antenna in both photon emitting and photon detecting devices. In addition, integration of optical antennas with optoelectronic devices can lead to the realization of highly compact multi-function platforms for future integrated photonics, such as low-cost lab-on-chip systems. In this review paper, we further focus on the effect of optical antennas on the detectivity of infrared photodetectors. One particular finding is that the antenna can have a dual effect on the specific detectivity: while it can elevate light absorption efficiency of sub-wavelength detectors, it can potentially increase the noise of the detectors due to the enhanced spontaneous emission rate. In particular, we predict that the detectivity of interband photon detectors can be negatively affected by the presence of optical antennas across a wide wavelength region covering visible to long wavelength infrared bands. In contrast, the detectivity of intersubband detectors could be generally improved with a properly designed optical antenna.

1. Introduction

The past decade has witnessed a rapid growth in the field of optical antennas, as they have proven to be an excellent tool for manipulating the propagation of light and its interaction with electrons in matter. The inherent abilities of optical antennas, combined with rapid advances in nanotechnology, have led to its widespread application in many (bio-)molecular sensing^{1, 2}, photonics^{3, 4} and optoelectronic devices^{5, 6}. At a more fundamental level, these devices can be divided into *passive* and *active* categories. Passive devices are inherently linear (e.g. flat optics⁷ and transformational optics⁸), while active devices are non-linear and incoherent (e.g. photodetectors^{9, 10}). Here, we focus on the application of optical antennas in active optoelectronic devices. The non-linear nature of active devices is responsible for their ability to amplify or transduce the optical signal, as well as to convert optical power to electrical power, or vice versa.

As we will see in the following, many interesting active optical devices have two major dimensional requirements: a large (microscale) optical component and a small (nanoscale) quantum absorber/emitter. The former is needed for efficient coupling of light to/from a distance, and the latter can significantly improve the sensitivity of the device. The dimension contrast is inherently related to the difference in photonic and electronic wavefunctions, and in the absence of a coupler, it results in a weak coupling between the two. The inefficient light-matter interaction can be enhanced using an optical antenna. Optical antennas can couple diffraction-limited far-field modes to sub-wavelength near-field modes in the vicinity of the nanoscale optical

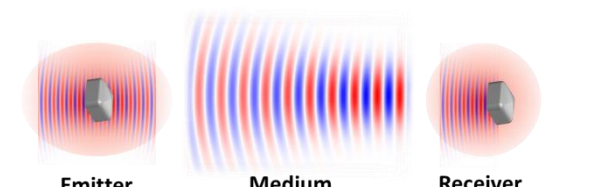
absorber/emitter. The sub-wavelength nature of the field near the antenna demands tight alignment, and hence there is a preference for direct integration of the antenna to the device.

The main motivations, a brief history, and the recent progress in integrating the optical antenna with the active optical device are the subjects of this review article. In section 2, a theoretical background is presented to explain the optical enhancement mechanism in the interaction between the far-field mode and the semiconductor nano-absorber/emitter. In section 3, we review two major categories of active devices with integrated optical antenna: light emitting and absorbing devices. However, the fundamental concept described in section 2 has been utilized in many other active devices, including modulators and switches¹¹.

2. Optical Antenna: Background and the Need for High Efficiency and Directivity

The weak interaction of light and matter is a double-edged sword: for example, it is responsible for our ability of chemical sensing and imaging across the universe, but on the down side, it severely limits the sensitivity of our detectors, as we will see in section 3.3. It is therefore highly desirable to be able to increase this interaction strength selectively and where needed. Naturally, since most optical systems take advantage of the large propagation distance of light, a high directivity is desirable. Table 1 shows some of the key parameters of the emitter, medium, and absorber for the case of infrared imagers. Details will be provided in section 3.3.1, but note that the conventional receiver (e.g., a piece of semiconductor) has a poor directivity compared to the incoming beam. Furthermore, the weak light-

matter interaction leads to a rather large absorption length, which demands a large volume of semiconductor to ensure high quantum efficiency (QE). In the following we shall see that the weak interaction can be substantially enhanced with a proper optical antenna design via an enhanced local density of states (LDOS). Although many commonly used optical antenna designs (e.g. Bowtie, Bulls-eye, Yagi-Uda, etc.) can produce a either a high QE or a high directivity, it is not easy to achieve both properties simultaneously. However, this is not a fundamental limit, and we will show a design based on photonic jets¹² that can achieve both requirements simultaneously. This method should be useful in many other applications, such as molecular sensing and solar harvesting, since their parameters are quite similar to those listed in Table 1.



Properties	Emitter	Medium	Receiver
Material	Thermally Excited Atoms-Molecules	Air	Semiconductor With Bowtie With Mettalo-dielectric
Light-Matter Interaction Length l (μm)	$\sim 10^2$	$\sim 10^9$	~ 10 ~ 1 ~ 1
Relative LDOS	~ 10	~ 1	~ 10 $\sim 10^2$ $\sim 10^3$
Radiation Directivity (dB)	~ 1.5	~ 20	~ 1.0 ~ 1.7 ~ 20

Table 1. Comparing optical properties of semiconductor integrated with different optical antenna.

2.1. Near-field and Far-field

An optical antenna is essentially a mode converter that can efficiently couple free-space propagative modes to spatially confined near-field modes. Fig. 1 illustrates the schematic of the optical antenna functionality. A sub-wavelength quantum emitter/absorber is similar to its classical counterpart, the electrically small dipole, and has a broad range of wave-vectors (due to the diffraction). This property leads to a spatial radiative beam with weak directionality. On the other hand, in many light trapping/extracting applications, the far-field optical mode is considered to be a propagative mode with high directionality consisting of a narrow range of wave-vectors. A highly directive antenna can establish efficient coupling between the wide-spread modes of the emitter/absorber, and the desirable directional far-field. Due to the reciprocity principle, the antenna can operate both as a receiver of, or transmitter to, the far-field. The antenna – emitter/absorber interaction is significant at the region near-field of the antenna, where the antenna modes are dominant compared with the free-space propagative modes. Antenna modes can be propagative or evanescent waves, and they carry radiative and non-radiative power, as well as store electromagnetic (EM) energy. These properties are often characterized by the antenna

quality factor and loss, as extensively discussed in the literature¹³. Antennas with large quality factor have low non-radiative and radiative antenna losses. At the first glance, the low radiative loss might seem to indicate a low coupling efficiency to the far-field. However, this is not true since the stored energy can be very large for antennas with large quality factor. In fact, a near unity coupling is possible, based on the coupled oscillator theory, but only at a very narrow spectral range. Since the minimum quality factor of the antenna is inversely proportional to its dimension (normalized to wavelength)¹³, one can conclude that broadband antennas cannot be optically small.

We conclude that highly efficient and broadband antennas with high directivity, which are most desirable for the aforementioned application, have to be optically large. All-metallic antennas based on adiabatic mode conversion can satisfy the above performance at the radio frequencies (e.g. horn antennas). However, large metal losses at the optical frequencies can significantly reduce the efficiency for an optically large, and all-metal optical antenna. This inherent limitations have motivated many research groups to develop metallo-dielectric hybrid antenna recently^{14, 15}.

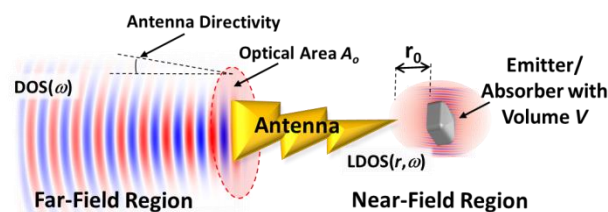


Fig. 1 Optical antennas couple far-field and the near-field, and enhance extracting light from a quantum emitter, or delivering it to a quantum load.

2.2. Local Density of States

In addition to the aforementioned mode coupling, an optical antenna can alter the photonic density of states (DOS) locally. This property could be utilized to increase radiative power from/to a quantum emitter/absorber. In vacuum, DOS is a function of photon frequency, $\text{DOS}(\omega) = \omega_0^2 / \pi^2 c^3$, and it determines the number of available photonic states that an electronic dipole can spontaneously emit to. However, the local density of state (LDOS) measures the geometrical and electromagnetic field effects on the locally available photon states by quantifying the electromagnetic energy density in the space and the polarization states. The value of LDOS for polarization state l can be defined as

$$\text{LDOS}_l(\mathbf{r}, \omega) = \sum_n \delta(\omega - \omega_n) (\epsilon(\mathbf{r}) |E_{n,l}(\mathbf{r})|^2 + \mu(\mathbf{r}) |H_{n,l}(\mathbf{r})|^2) \quad (1)$$

where, E_n and H_n are orthonormal eigenfields. In the case of a cavity with a quality factor Q , $\delta(\omega - \omega_n)$ the function can be approximately replaced by a Lorentzian spectrum with $\Delta\omega = \omega/Q$ ¹⁶. The total DOS is the volume integration over space and

summation over the polarization of LDOS, normalized to the volume of the space¹⁷:

$$\text{DOS}(\omega) = \frac{1}{V} \sum_{l=1}^3 \int \text{LDOS}_l(\mathbf{r}, \omega) d^3r \quad (2)$$

Importantly, the spontaneous emission rate of a dipole is proportional to the LDOS,

$$\Gamma_{sp} = \frac{\pi\omega_0}{3\epsilon_0\hbar} |\langle a|\hat{\mu}|b\rangle|^2 \text{LDOS}(\mathbf{r}_0, \omega_0) \quad (3)$$

where, $\mu_{ba} = |\langle a|\hat{\mu}|b\rangle|$ is the dipole moment.

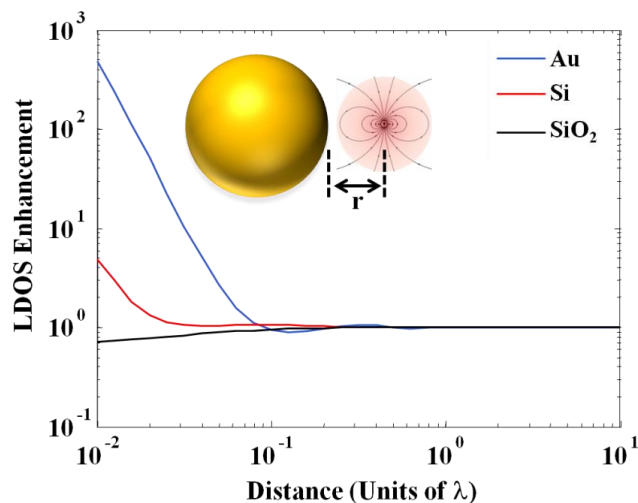


Fig. 2 LDOS as a function of distance from a 100-nm-diameter nanosphere for three different materials: metal (Gold), semiconductor (Si) and insulator (SiO₂) and at a wavelength of $\lambda=500$ nm.

Thus, the LDOS distribution in space determines the radiation enhancement/suppression due to the presence of polarizable objects such as optical antenna. Fig. 2 shows the LDOS as a function of distance from a sphere with a 100 nm diameter, and made with three different materials.

Although LDOS is an important property of the microcavities, optical antennas and other photonic structures, a straightforward and universal definition of LDOS in a *dissipative* system has been subject to many debates and controversies for decades¹⁸⁻²⁴. In practice, almost all materials in nature exhibit a certain level of optical loss. Specifically, in light trapping/extracting applications such as photodetector and LED devices, considering the loss of the active region is crucial for proper evaluation of LDOS. It should be emphasized that the definition of LDOS in equation (1) is under the lossless condition, where eigen-modes are Hermitian and orthogonal¹⁷, allowing the LDOS to be derived from the converging imaginary part of the system's Green's function^{25,26}. However, in a lossy system a set of orthogonal eigen-modes no longer exists to define LDOS as in equation (1)²⁶. In addition, insertion of loss mixes both real and imaginary parts of Green's function, leading to the divergence of the imaginary part²⁷. In general, there are two major approaches to resolve LDOS calculation issues in lossy systems. The first approach is to circumvent the divergence issue of the imaginary part of Green's function, for example by introducing locally lossless homogeneous medium at the dipole position where LDOS is to be calculated¹⁴. The second approach is to redefine the LDOS formalism, for example by introducing a small set of quasi-

normal modes²⁶, or replacing delta function by a finite line-width Lorentzian function¹⁷. In this paper, the latter approach is chosen to calculate LDOS at a dissipative medium. This approach is highly compatible with finite-difference-time-domain method.

In the same vein, circuit theory could be used to model and optimize optical antennas. Using this approach, it becomes evident that the impedance of the quantum emitter/absorber is quite different from the vacuum impedance. Antenna can adjust the impedance mismatch problem by behaving as an impedance matching circuit^{28,29}.

3. Integration of Optical Antenna with Active Devices

3.1. Semiconductor Lasers with Integrated Optical Antenna

Integrated optical antennas on laser sources have many advantages, since they directly modify the near-field and far-field properties of the lasers' beams. Many applications could significantly benefit from such a modification, including microscopy, spectroscopy, nanoscale optical lithography, heat assisted magnetic recording, spatially resolved chemical imaging, and laser processing. The integration of optical antennas with lasers can be categorized into the far-field and the near-field modification of the lasers' output. Far-field modification of laser outputs is the goal of a large volume of research, such as optical data recording, far-field optical microscopy, and laser beam shaping and collimation. On the other hand, near-field modification is mainly used for biological spectroscopy and molecular sensing, since it provides great field enhancement at the near-field of an optical antenna. In the following, we look at the major achievements in both areas.

3.2.1. Laser far-field modification

The initial motivation for the integration of the optical structure with a laser to modify its far-field goes back to the research efforts to reduce laser spot size in optical data recording technologies^{30, 31}. As an example, early work demonstrated the recording of 250-nm-diameter marks at 7.5 Gb/in² by fabricating a very small aperture laser (VSAL) operating at $\lambda = 980$ nm with a 250-nm-square aperture at the facet of the laser³⁰. VSAL was further investigated to realize a high-resolution far-field scanning optical microscope by controlling the focal length of the transmitted field's spot^{32, 33}. A main parameter in the evaluation of the quality of the laser beam at the far-field, in terms of divergence and directionality, is the directivity of the optical structure fabricated on the laser's facet. An aperture on the facet of a laser cannot enhance the directivity of the beam in the far-field, instead, it modifies the field's spatial distribution by the aperture's Fourier transformed shape. Directivity enhancement can be achieved by coherent interference between an array of optical elements and apertures, similar to a phased array antenna in RF terminology³⁴⁻³⁷. For example, *B. Guo et al.* fabricated an optical antenna on a 650-nm-wavelength commercial laser, which was consisted of a 300x500 nm² aperture and four concentric rings to focus the beam $\sim 2\lambda$ away from the laser's facet with a 140% intensity enhancement³⁵. An edge-emitting semiconductor laser has an intrinsic beam divergence that limits the coupling efficiency of the beam to optical fibers and waveguides. Using an aperture-groove optical antenna on a quantum cascade laser

(QCL) at $9.9\ \mu\text{m}$, *N. Yu et al.* reported ~ 25 times reduction in the beam spreading. The interference of the light radiated from the aperture with the light scattered by the 1D-grooves reduces the divergence angle to as little as 2.4 degrees in the direction of the grooves, and increased the beam directivity by at least 10 dB³⁷.

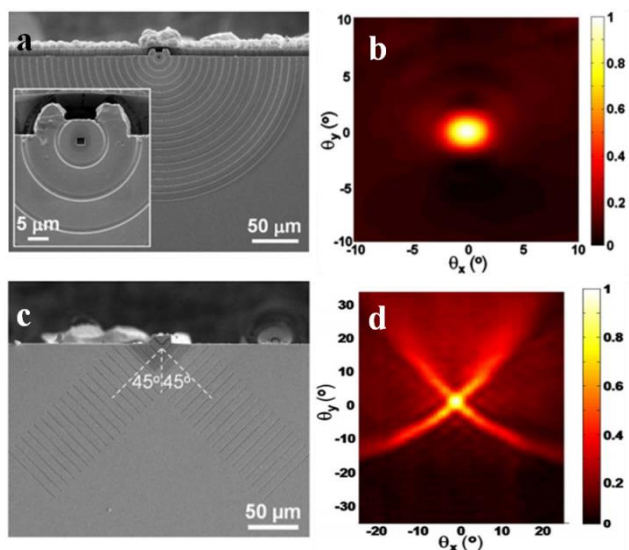


Fig.3 Far-field modification using optical antenna integrated with quantum cascade lasers (QCL). a-b) SEM image of concentric grooves with aperture on QCL, and the measured far-field of the output laser. Reproduced with permission of the American Institute of Physics from ref. 38. c-d) SEM image of two set of aperture-grooves on QCL, and the measured far-field that produces a combination of linear and circular polarization. Reproduced with permission of the American Institute of Physics from ref. 42.

In order to collimate light cylindrically, concentric grooves have been implemented (Fig. 3a-b)³⁸. Additionally, the superposition of concentric rings results in multiple collimated beam generation in the far-field^{39,40}. The same group has reported a similar optical antenna integrated on a high power QCL laser to collimate the far-field beam⁴¹. Since the orientation of the grooves determines the polarization of scattered light from individual grooves in the far-field, the polarization of the laser can be rotated relative to the groove orientation. For example, the combination of two sets of aperture-grooves, tilted 45 degrees in opposite directions can produce a combination of linear and circular polarization⁴² as shown in fig. 3c and d. The concept of optical antenna integration on semiconductor lasers is also adapted to THz laser sources utilizing spoof plasmonics⁴³ and concentric circular grating⁴⁴.

3.2.2. Laser near-field modification

Many applications, such as molecular sensing and low power switching, can greatly benefit from a laser beam that is tightly confined within a sub-wavelength volume. Very large confinements can be accomplished in the near-field, where evanescent modes exist. Although sub-wavelength apertures on facets of lasers can confine light, the coupling of the laser cavity modes to the near-field is very inefficient,⁴⁵ since the optical transmission through a sub-wavelength aperture decays rapidly (it is proportional to the fourth power of the aperture size)⁴⁶. Unlike tiny apertures, optical antennas can efficiently convert laser power to the near-field and reduce the power loss. The first demonstration of optical antenna integration on an edge emitting

laser was reported by *E. Cubukcu et al.*⁴⁵ where a coupled nanorod antenna was fabricated on the facet of a commercial near-infrared laser using focused ion beam (FIB) milling.

The application of such integrated optical antennas has been extended to biological imaging and spectroscopy by fabricating an integrated system in the mid-infrared region, where many biological and chemical molecules have absorption features⁴⁷⁻⁵². This integration of optical antennas with active devices could propel lab-on-chip technology one step closer to fully integrated microsystems⁵³. Recent progresses in QCLs have led to realization of lasers with excellent properties in the mid and long infrared regions, where many important biomolecules have strong absorption features. However, biomolecules' overall optical absorption is still very weak in their naturally occurring concentrations. Since mid and long-wave infrared detectors have a poor sensitivity at room temperature, the aforementioned weak absorption cannot be detected with a system operating at room temperature. One of the ideas we developed to address this issue was to take advantage of the laser's non-linearity near its threshold and the strong coupling between the laser cavity mode and the optical antenna mode.

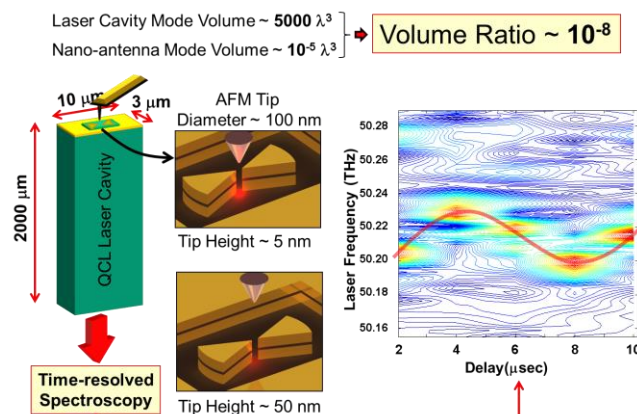


Fig. 4 The schematic of an integrated bowtie antenna with a QCL (left). Using time resolve spectroscopy (right), we measured the frequency shift and intensity of QCL laser due to the mechanical motion of an atomic force microscope (AFM) tip (center). Despite the extremely large volume difference between the antenna modes and laser cavity modes (about 10^{-8}), as well as the sub-wavelength motion of the AFM tip of $\sim \lambda/120$, laser output is strongly modulated by the tip motion.

We initially fabricated and measured single⁴⁹ and coupled metal-oxide-metal antennas⁴⁸ on the facet of QCLs operating near $\lambda \sim 6\ \mu\text{m}$. Our experiments suggested that the perturbation of antenna's hot-spot can affect the laser dynamic due to the strong coupling of the antenna and cavity modes. We then demonstrated strong modulation of QCL cavity modes by perturbing the integrated optical antenna's near-field through an atomic force microscope (AFM) tip movement⁵⁴. In this work, a non-linear feedback mechanism was shown to enhance the sensitivity in detecting molecules in the proximity of antenna. Fig. 4 shows a schematic of a bowtie antenna integrated on the facet of a QCL, and the relative position of the AFM tip. The AFM is operated on a non-contact mode with an amplitude oscillation of $\Delta d = 50\ \text{nm}$ near the antenna hot-spot. As a result of AFM tip movement by about $\lambda/100$, laser power is modulated by $\sim 74\%$, and its frequency shifts by $\Delta f \sim 30\ \text{GHz}$. The figure of merit (FOM) of

the frequency tuning of the laser in this experiment is $g = \Delta f/\Delta d \sim 6.4 \times 10^8 \text{ Hz.nm}^{-1}$, as shown in our time-resolved spectroscopy measurement (see Fig. 4). The measured FOM shows the extremely high modulation of laser operation caused by perturbing the antenna hot-spot due to the concentration of EM energy in the high LDOS in the antenna's near-field. The resultant FOM is about 10 times larger than the best results achieved by modifying the cavity modes mechanically⁵⁵. More importantly, the volume of the moving part in our approach is about five orders of magnitude smaller.

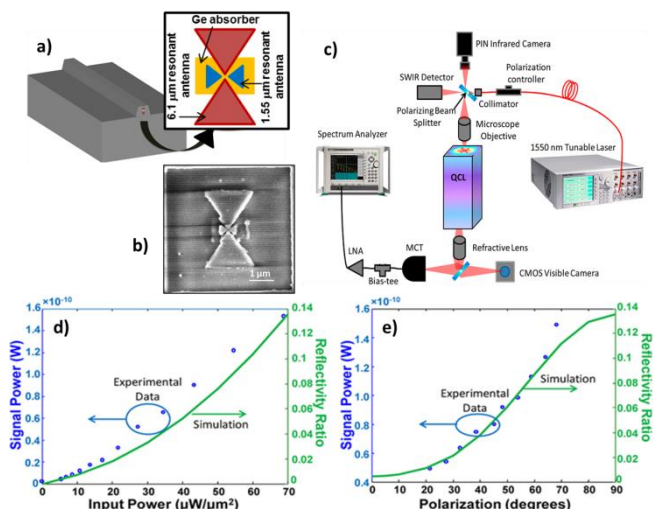


Fig. 5 a) Schematic and b) SEM image of a cross-polarized optical antenna operating at 1.55 μm and 6 μm Integrated on QCL laser. c) Schematic of the setup to measure the near-field and modulation field of the laser. d) Modulation of back-reflection 6- μm -wavelength power from QCL laser as a function of 1.55- μm -wavelength pumping power, e) as a function of 1.55- μm -wavelength polarization.

Another interesting feature of an optical antenna is its ability to confine electromagnetic fields into a hotspot almost independent of its wavelength. This property allows coinciding optical beams with very different wavelengths on nonlinear media. Such a feature can be utilized for ultra-fast and low-power switching, wavelength mixing and converting by means of a nonlinear element in the system. As an example, we reported dynamic control of the near-field using a cross-polarized optical antenna integrated on a QCL laser⁵⁶. The optical antenna is composed of two Bowtie antennas resonating at 1.55 μm and 6 μm as shown in Fig. 5a. A thin slab of germanium is fabricated at the antenna gap as the nonlinear element. The near-field of a 6- μm -wavelength QCL laser is controlled through free carrier absorption induced in germanium by a 1.55- μm -wavelength pumping light. The modulated, back-reflected signal from the laser is detected by an MCT detector before it is sent to a spectrum analyzer. Fig. 5e and f show the emitted power of the QCL laser at $\lambda \sim 6 \mu\text{m}$ modulated by a weak laser beam at 1.55 μm . The power dependency of the QCL emission to the polarization of the short wavelength beam clearly demonstrates the antenna's role.

3.2. Semiconductor LEDs with Integrated Optical Antennas

One of the main limitations of light emitting diode (LED) is its low external quantum efficiency. This is partly due to the limited light extraction efficiency, which is the percentage of light that can leave the semiconductor and couple to the propagative optical

modes. The second limiting factor is the small spontaneous radiation rate that allows other non-radiative mechanisms to consume a portion of the energy. Enhancing light extraction efficiency has been an intense field of research and different solutions have been developed. For example, using micro-lenses and micro-structuring the semiconductor it has been enhanced by about one order of magnitude⁵⁷. However, in order to reach the luminosity of fluorescent lamps or light bulbs, significant improvement is necessary for LEDs⁵⁸. The motivation for the integration of optical antennas with LEDs is the desire to increase light emission from LEDs beyond the limited enhancement of conventional photonic methods. In early 1990, A. Kock *et al.* reported the first strongly directional emission from an infrared AlGaAs/GaAs surface-emitting LED via coupling to the surface plasmons⁵⁹. They used a surface grating that acted like an antenna and provided efficient coupling of emitted photons from an electronic dipole to the far-field. It also enhanced the optical density of states, and subsequently, the spontaneous emission rate in the semiconductor⁶⁰. In 2004, K. Okamoto *et al.* reported considerable light emission improvement from InGaN/GaN quantum wells, which were coated with plain and perforated thin films of silver⁵⁸. Since then, a variety of antenna configurations are fabricated on the facets/surfaces of LEDs with different materials and emitting wavelengths⁶¹⁻⁶³. The most challenging issue in using metallic antenna in this application is the large metal loss in the visible spectrum⁶⁴.

3.3. Semiconductor Photodetectors with Integrated Optical Antennas

Fast photodetectors with high sensitivity and quantum efficiency are key elements in many modern applications, such as optical communication, optical interconnects, quantum key distribution and infrared imaging. It is therefore crucial to optimize the quantum efficiency-bandwidth product while maintaining a low noise. Traditional photon detectors are optimized based on planar device geometry, where the optical (collection) area and the electrical (sensing) area are equal. Although increasing the material volume can increase the absorption, and hence the QE, the detector's overall performance is degraded by increases in power loss, latency, and noise⁹. In many conventional photodetectors, the device speed is limited by the carrier transit time, and a shorter transit time requires a thinner active region. Moreover, a thinner active region has smaller volume and hence a smaller dark current (noise). Unfortunately, a thinner active region means a smaller QE. A common approach to shrink the device size while maintaining a high QE is to use resonant cavities^{65, 66}. However, this approach can severely limit the optical bandwidth of the detector.

The main motivation in integrating optical antenna with photodetector is the need to surpass the aforementioned limitations and produce a very small (deep sub-wavelength) absorber with high QE, high directivity, high sensitivity (detectivity), and a broad optical bandwidth. As we saw in section 2, optical absorption (QE) can be significantly enhanced in the presence of an optical antenna, due to the elevated LDOS. Unlike micro-cavities, this enhancement can be very broadband. Fortunately, optical antennas are quite efficient at longer wavelengths (due to the lower metal loss), and this is in fact the region that the semiconductor optical absorption is weaker⁶⁷.

While the above idea has recently been studied by many groups, the effect of LDOS enhancement on the detector noise is commonly ignored. In section 2.2, we saw that LDOS enhancement leads to an increased radiative recombination rate, which leads to an increased generation rate due to the detailed balance principle. The increased carrier generation rate produces higher noise in the detector. This effect could be particularly significant for interband detectors, where the carrier lifetime is quite long⁶⁸. In order to calculate the sensitivity, we need to calculate the noise and the signal of the detector. The noise current, in both interband and intersubband photodetectors, is $I_n = qg\sqrt{2V(G+R)BW}$, where $V=A_e t$ is the electrical volume of the detector, A_e and t are the semiconductor area and thickness, g is the internal gain, and G and R are the generation and recombination rates. For a device operating near equilibrium we have $G \cong R$. The net recombination rate is the sum of the radiative and non-radiative recombination rates: $R = R_{rad} + R_{non-rad}$. The photodetector signal, or current responsivity, is $R_i = \eta qg\lambda/hc$, where η is the quantum efficiency (QE), and λ is the wavelength of the light. The device detectivity (sensitivity) is the signal to noise ratio, normalized for area and bandwidth: $D^* = R_i/I_n\sqrt{A_o BW}$, where A_o is the optical (collecting) area of the device. Assuming equal optical and electrical areas (i.e. conventional photodetectors), the optimum detector thickness is found to be $t_{opt} = 1.26/\alpha$, leading to the highest possible sensitivity of $D_{max}^* = 0.31\lambda/hc\sqrt{\alpha/R}$, where α is the semiconductor absorption coefficient.

This has been the sensitivity limit of conventional photodetectors for the past few decades. Now we would like to see if optical antennas can help us exceed the above sensitivity limit. In this analysis, we assume that the beam is already focused to a diffraction-limited spot using conventional optics with an NA~1 (i.e. the practical focusing limit in the air). The optical area is then $A_o \sim \lambda_0^2/\pi NA$.

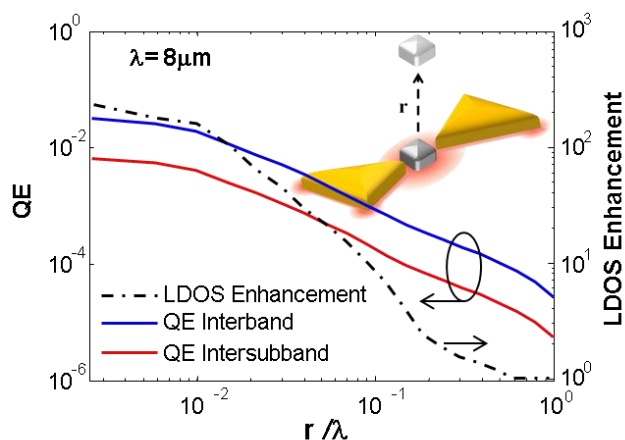


Fig.6 a) LDOS enhancement, and QE of sub-wavelength interband and intersubband absorbers with volume $V=3.1 \times 10^{-5} \lambda^3$, as a function of distance r from the center of a bowtie designed for $\lambda=8 \mu\text{m}$.

First, we find the detectivity of a deep sub-wavelength detector with volume $V \ll \lambda^3$ without any antennas to be $D_0^* \sim 0.5 \alpha/hc \sqrt{\pi V/R}$. As expected, the detectivity degrades for smaller device volumes, since the signal decreases at a faster pace than the noise.

Now we would like to see whether we can increase the QE and detectivity of a deep sub-wavelength detector using antennas. Since LDOS enhancement is highly dependent on the geometry and configuration of the antennas, it is not possible to develop a general formalism. Therefore, we will quantify this effect by using two examples: a widely used Bowtie antenna, and a metallo-dielectric hybrid antenna we recently proposed¹². The bowtie antenna does not produce a large QE and is not directional, while the hybrid antenna can produce a much higher QE and directivity. However, we will see that the performance in each case strongly depends on whether an interband or an intersubband sub-wavelength detector is used.

Both antennas are optimized for detection at $\lambda=8 \mu\text{m}$. The detector dimension is $400 \text{ nm} \times 400 \text{ nm} \times 100 \text{ nm}$ for the bowtie, and $1 \mu\text{m} \times 1.5 \mu\text{m} \times 2 \mu\text{m}$ for the hybrid antenna. The real part of the semiconductor refractive index is assumed to be about 3, and the absorption coefficients are assumed to be 1000 cm^{-1} for the intersubband and 5000 cm^{-1} for the interband absorber⁶⁷. As mentioned in section 2.2, LDOS calculation in the presence of lossy medium is not a well-defined problem and is an open subject for researchers. In this paper, finite-difference time-domain (FDTD) method was used to calculate the LDOS at the absorber site using¹⁷:

$$\text{LDOS}_l(x_0, \omega) = \frac{4}{\pi} \epsilon(x_0) P_l(x_0, \omega) \quad (4)$$

where, $P_l(x_0, \omega)$ is the radiative power from a dipole that is placed at x_0 and has the polarization state l . Since the system is dissipative due to the optical absorption of the semiconductor, the radiative recombination can decay into a finite range of frequencies. Thus, the total LDOS is calculated by integration over all the frequencies weighted by a Lorentzian lineshape for their contribution¹⁷.

$$\text{LDOS}(x_0) = \int \frac{1}{\epsilon(x_0)} \text{LDOS}_l(x_0, \omega) \frac{\gamma_0/\pi}{(\omega-\omega_0)^2 + \gamma_0} d\omega \quad (5)$$

This approach ensures the non-radiative decay of dipole due to the dissipative host is taken into account by γ_0 . The value of the QE is calculated from the net power dissipated by the absorber, normalized to a Gaussian source with numerical aperture NA=1 (corresponding to $A_o \sim \lambda_0^2/\pi NA$). Fig. 6 shows QE and LDOS enhancement as a function of distance r between the detector and the Bowtie antenna gap. In this geometry, LDOS and QE monotonically increase as r approaches zero, signifying the optical antennas role in enhancing the spontaneous emission and far-field power absorption in the semiconductor absorber. Although the bowtie antenna enhances QE significantly, the maximum value is still around 1%. Also, the bowtie directivity is quite dismal (~2 dB). On the contrary, the hybrid antenna can produce a high QE of about 50% and a high directivity (~20 dB) simultaneously¹².

Now we would like to compare the detectivity of interband and intersubband detectors integrated with each antenna, and compare them to the conventional values at $\lambda=8 \mu\text{m}$. The main question is whether a high LDOS produced by the bowtie and hybrid antennas (~230 and 1100 times vacuum level respectively) can adversely affect their detectivity due to the reduced radiative lifetime.

Fig.7 shows the calculated detectivity for the above antennas

for the two cases of interband and intersubband absorbers. For interband, we used the parameters⁶⁸ of $\text{Hg}_{1-x}\text{Cd}_x\text{Te}$ (MCT) with a cutoff wavelength of around $8\ \mu\text{m}$ ($x\sim 0.22$). For intersubband we used the parameters⁶⁷ of AlGaAs QWIP with a peak detection wavelength of $8\ \mu\text{m}$. The background-limited performance (BLIP) detectivity is also shown in this figure. It is evident that the detectivity of hybrid antennas integrated with the QWIP is more than 30 times higher than the limit of conventional QWIP detectors at all temperatures. The value of $\text{QE}\sim 40\%$ is also quite large. However, the optical antennas could not increase the detectivity of the interband detector beyond the limit of conventional devices. The reason is the comparable radiative lifetime τ_{rad} and non-radiative lifetime $\tau_{\text{non-rad}}$ in interband detectors. For example, the ratio of the radiative to non-radiative lifetime in the MCT is around 0.1 at $T=77\ \text{K}$, and 25 at room temperature. However, LDOS enhancements of 230 for the bowtie antenna means that the new radiative recombination lifetime is about ten times *smaller* than the non-radiative lifetime even at room temperature. Therefore the noise of the detector integrated with the antenna is dominated by the enhanced radiative noise at any temperature. For the QWIP however, $\tau_{\text{rad}}\sim 1\ \mu\text{s}$ and $\tau_{\text{non-rad}}\sim 200\ \text{ps}$ at $T=77\ \text{K}$ ⁶⁹, and hence the ratio is about 5000. This large ratio means that the LDOS enhancement, even for the hybrid antenna, cannot enhance the detector noise at any temperature. This conclusion is valid for the mid and long wavelength infrared interband and intersubband detectors ($3\ \mu\text{m} < \lambda < 12\ \mu\text{m}$). In the shorter wavelength bands, where intersubband detectors are not commonly used, their performance might be limited by the LDOS enhancement. In the very long wavelength infrared (VLWIR) and terahertz (THz) region, where interband devices are not commonly used, LDOS enhancement will not produce the aforementioned limit. Therefore, this analysis suggests that optical antennas integrated with interband devices in these spectral bands have a lot of unexplored potential. Let us now look at the state-of-the-art in each interband and intersubband category.

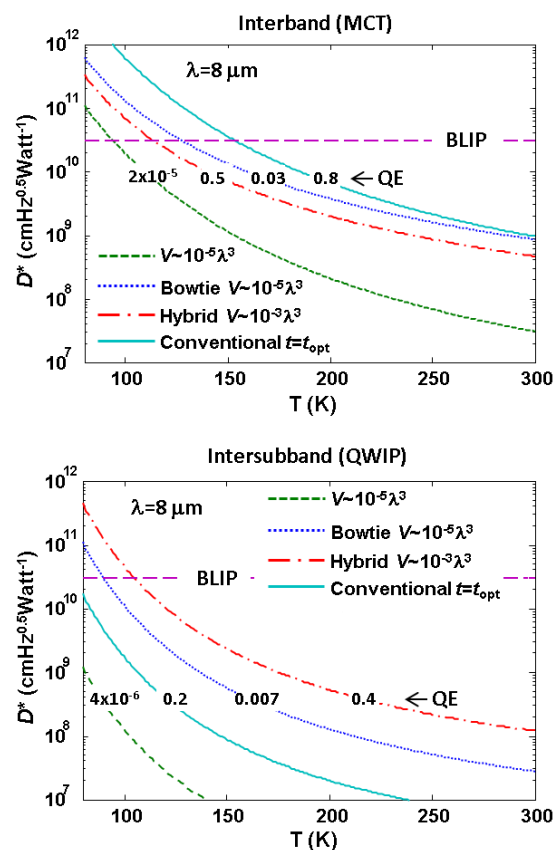


Fig.7. Detectivity versus temperature for interband (top) and Intersubband (bottom) absorbers. The plots compare detectivity and QE for four cases: a deep sub-wavelength absorber, bowtie and hybrid antennas integrated with sub-wavelength absorbers, and a conventional detector with optimum thickness. Optical antennas dramatically enhance detectivity of the intersubband devices and surpass the limit of conventional device by ~ 30 times, but their LDOS enhancement prevents detectivity improvement for the interband devices.

3.3.1. Optical Antennas Integrated with Interband Photodetector

In a pioneering work, *L. Tang et al.* reported a metal-semiconductor-metal (MSM) germanium (Ge) detector with a deep sub-wavelength dimension $\sim \lambda^3/10000$ integrated with a half-wave Hertz dipole antenna⁹. The extremely small volume suggests a high speed operation of $\sim 100\ \text{GHz}$, as well as a very small capacitance. The latter is particularly important as a large load resistance can be used to generate a high output voltage and very low optical and electrical power consumption for on-chip optical interconnects. The performance enhancement of MSM photodetectors has been the subject of much research⁷⁰⁻⁷⁷ due to their relative low cost of fabrication and compatibility with CMOS technology⁷⁰. The detector's electrodes, used for extracting the current, can serve as optical antennas to capture and focus light efficiently at the detection site. For example, *F. Ren et al.* reported an integration of a split-ring bull's eye antenna on a germanium detector⁷². The bull's eye antenna focuses light from a relatively large area (with a diameter of $\sim 10\lambda$) into a subwavelength germanium slab resulting in an enhancement of the LDOS and electric field. The measured photocurrent is improved by a factor of 7 with a responsivity of $\sim 3.93\ \mu\text{A/W}$. *P. Fan et al.* have fabricated the electrodes of a germanium

nanowire to capture light from the far-field and concentrate it on the germanium nanowire⁷¹. The nanowire has optical resonant modes that can coincide with the contact antenna's resonance wavelength resulting in ~ 1.7 times enhancement of polarization-dependent optical absorption in germanium at 660-nm-wavelength. Combining a resonant micro-cavity with an optical antenna increases the photon interaction time at the detection site, in addition to the efficiency of the far to near-field coupling. *K. Balram et al.* have reported a hybrid micro-cavity optical antenna that strongly enhances the optical absorption in a germanium detector below the bandgap with a measured responsivity of ~ 1.2 A/W. The micro-cavity antenna consists of a planar metal-dielectric resonant cavity⁷⁰. The electrodes adjacent to the germanium create a cavity in the germanium region. The cavity size (germanium width) is tailored in order to excite the highest Q mode (5th cavity mode) to increase the photon interaction time in the cavity. In addition, changing the germanium's width will shift the wavelength of the cavity mode, which changes the detection wavelength adding a tuning feature to the detector. The same group has reported a similar structure with a MSM deep sub-wavelength silicon photodetector operating at the near-IR region⁷⁴. The demonstrated MSM silicon photodetector has the tuning feature due to the micro-cavity antenna, which is favourable for applications such as multispectral imaging sensors and short-range optical interconnects.

3.3.2. Optical Antennas Integrated with Intersubband Photodetector

Photodetectors based on the intersubband absorption of photons in quantum wells have two distinct features when compared with interband detectors: a high non-radiative recombination rate due to the fast LO phonon scattering between the subbands, and high polarization sensitivity due to the quantum well transition selection rule. Since quantum wells are usually separated by rather thick barriers, and a relatively small dipole matrix, the overall optical absorption coefficient of intersubband detectors is considerably smaller than interband detectors. The shorter carrier lifetime and smaller optical absorption coefficient means that the detectivity of intersubband detectors is fundamentally lower than that of interband detectors. However, the technological advantages of intersubband detectors—particularly at the longer infrared wavelength range. As we discussed in section 3.3, the effect of optical antennas is more significant for intersubband mid- and long wavelength infrared photodetectors, where the weak optical absorption results in a QE of about 20% in conventional devices. In 2010, we reported¹⁰ an ultra-thin ($\lambda/16$) QWIP integrated with a nanohole-array optical antenna to produce a high QE of $\sim 40\%$ (see Fig. 8a and b). The top view of the $|E_z|^2$ at the nanohole-array/detector interference and simulated with FDTD, as well as the side view of $|E_z|^2$ through the quantum well's growth direction are shown in Fig. 8c and d. The responsivity and detectivity of this device are shown in Fig. 8e. The optical antenna captures far-field light and enhances its concentration at the active region of the QWIP. In addition, the QWIP can only absorb light with a polarization perpendicular to the growth direction. The nanohole-array antenna converts the lateral polarization of light to a perpendicular polarization by exciting the surface plasmons on the surface of the perforated metal. Fig. 5b shows the simulated

electric intensity with a polarization perpendicular to the QW growth direction. The peaks of responsivity and detectivity both occur at 8 μm , reaching ~ 7 A/W and $\sim 7.4 \times 10^{10}$ $\text{cmHz}^{1/2}/\text{W}$ respectively. A similar far-field to near-field coupling property of periodic hole-arrays has been reported without using surface plasmons. In this work, a QWIP operating at 7.6 μm was integrated with a hexagonal air-hole array. Although a similarly high enhancement could be produced with this micro-resonator photonic crystal QWIP, the high Q factor of about 135 led to an extremely narrow detection bandwidth⁷⁸.

Nanohole-array optical antennas have been used to enhance quantum dot infrared photodetectors (QDIPs)⁷⁹ as well, with about five times enhancement in the responsivity and the detectivity. In addition, a focal plane array (FPA) of nanohole optical antennas integrated on a QDIP has been reported with 15 times greater detectivity at 8.3 μm wavelength⁸⁰.

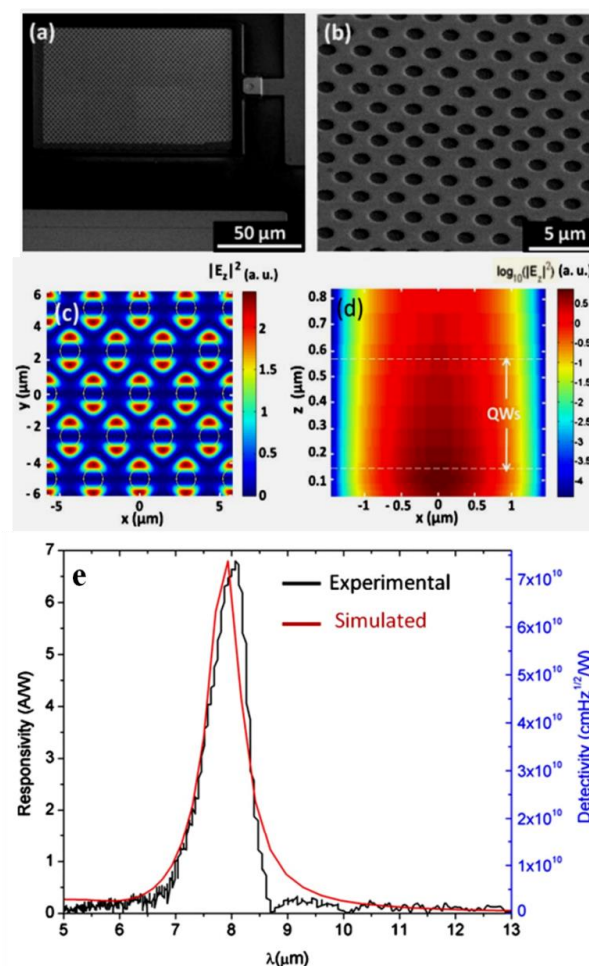


Fig. 8 a) SEM images of nanohole array optical antenna integrated on a QWIP photodetector. b) Map of FDTD simulated $|E_z|^2$ at the bottom of nanohole array antenna, c) along the quantum well's growth direction. d) The measured responsivity of the device at bias 0.7 V at 78 K and the spectrum of average $|E_z|^2$ in the active region. Reproduced with permission of the American Institute of Physics from ref. 10.

Although, nanohole array antenna enhances the photodetector performance, it only confines light in one dimension. Similar to the MSM Ge integration with micro-cavity antenna, incorporation of micro-cavity property with far-field-to-near-field coupling can

increase the light-matter interaction as well as allows reducing the detection volume in deep sub-wavelength scale. Recently, a double-metal nanoantenna as micro-cavity has been fabricated on a QWIP detector to confine light 3-dimensionally⁸¹. Strong sub-wavelength light confinement of this micro-cavity antenna leads to three times reduction in dark current, due to the reduced detection area. As described in the section 3.3, we recently proposed a novel hybrid optical antenna¹² that can achieve a similarly higher QE, but at smaller volumes. In addition, it can produce a large directivity. The simulated QE is ~50% and directivity gain of ~16 dB has been achieved in a QWIP active region with a volume of ~0.006 λ^3 . A recent simulation of another type of metallo-dielectric optical antenna⁸² suggests that large QE of over 85% with extremely large emission rate enhancements of LDOS~3000 is possible for single dipole emitter/absorber.

4. Conclusion

In this paper, we reviewed the recent progress and developments in optical antennas integrated with active optoelectronic devices, such as lasers, LEDs, and photodetectors. Theoretical and experimental works suggest that such devices have the potential to address many of the inherent limitations of conventional optoelectronic devices. In particular, they have two significant capabilities: they can enhance both the local density of states and the coupling of the near-field modes to the far-field modes. Many devices utilizing these capabilities to achieve enhanced efficiency and sensitivity have successfully been demonstrated. However, the enhancement of the light-matter interaction does not necessarily lead to increased sensitivity. We showed that the sensitivity of detectors could even degrade with the addition of optical antennas, if their noise is already limited by the radiative generation of carriers.

Historically, the strong light-matter coupling produced by optical cavities in the field of cavity quantum electrodynamics (CQED), has led to significant fundamental and practical discoveries⁸³ as signified by the 2012 Nobel Prize in Physics. However, the required high quality factor of such cavities makes it difficult to achieve a fast interaction time. On the contrary, optical antennas have the ability to enhance the light-matter coupling at nano-scale dimensions, and at ultrafast time scales⁸⁴. These unique abilities could potentially lead to significant fundamental and practical breakthroughs. Recent experimental demonstrations, such as ultrafast optical spectroscopy of nanoparticles⁸⁵ and nano-spectroscopic imaging⁸⁶, suggest that rapid progress in this field has already started. In parallel, the unique properties of optical antennas have excellent synergy with the properties new 1D and 2D active devices, such as carbon nanotube and graphene. Early demonstrations in this area⁸⁷⁻⁸⁹ are indicative of a paradigm shift in the field of nano-optoelectronics. On a broader scale, we believe that the impact of integrated optical antennas on many technologies, including ultra-sensitive compact medical sensors and ultra-fast on-chip optical interconnects is imminent.

Acknowledgement

This work is partially supported by ARO through award # W911NF-11-1-0390, and NSF through award # ECCS-1206155

and # ECCS-1310620.

References

1. A. Kinkhabwala, Z. Yu, S. Fan, Y. Avlasevich, K. Müllen and W. Moerner, *Nature Photonics*, 2009, 3, 654-657.
2. N. Liu, M. L. Tang, M. Hentschel, H. Giessen and A. P. Alivisatos, *Nat. Mater.*, 2011, 10, 631-636.
3. J. B. Lassiter, H. Sobhani, J. A. Fan, J. Kundu, F. Capasso, P. Nordlander and N. J. Halas, *Nano letters*, 2010, 10, 3184-3189.
4. N. Liu, L. Langguth, T. Weiss, J. Kästel, M. Fleischhauer, T. Pfau and H. Giessen, *Nat. Mater.*, 2009, 8, 758-762.
5. M. W. Knight, H. Sobhani, P. Nordlander and N. J. Halas, *Science*, 2011, 332, 702-704.
6. K. Ding and C. Ning, *Light: Science & Applications*, 2012, 1, e20.
7. N. Yu, P. Genevet, F. Aieta, M. Kats, R. Blanchard, G. Aoust, J. Tetienne, Z. Gaburro and F. Capasso, 2013.
8. H. Chen, C. Chan and P. Sheng, *Nat. Mater.*, 2010, 9, 387-396.
9. L. Tang, S. E. Kocabas, S. Latif, A. K. Okyay, D.-S. Ly-Gagnon, K. C. Saraswat and D. A. Miller, *Nature Photonics*, 2008, 2, 226-229.
10. W. Wu, A. Bonakdar and H. Mohseni, *Applied Physics Letters*, 2010, 96, 161107-161103.
11. A. Bonakdar, J. Kohoutek, D. Dey and H. Mohseni, *Opt Lett*, 2012, 37, 3258-3260.
12. A. Bonakdar and H. Mohseni, *Opt. Lett.*, 2013, 38, 2726-2728.
13. M. Agio, *Nanoscale*, 2012, 4, 692-706.
14. L. Yousefi and A. C. Foster, *Opt Express*, 2012, 20, 18326-18335.
15. A. Ahmed and R. Gordon, *Nano Letters*, 2012, 12, 2625-2630.
16. A. F. Koenderink, *Opt Lett*, 2010, 35, 4208-4210.
17. A. Taflove, S. G. Johnson and A. Oskoobi, *Advances in FDTD Computational Electrodynamics: Photonics and Nanotechnology*, Artech house, 2013.
18. S. Scheel, L. Knoll and D. G. Welsch, *Phys Rev A*, 1999, 60, 4094-4104.
19. S. M. Barnett, B. Huttner and R. Loudon, *Phys Rev Lett*, 1992, 68, 3698-3701.
20. H. T. Dung, L. Knoll and D. G. Welsch, *Phys Rev A*, 2000, 62.
21. G. Juzeliunas, *Phys Rev A*, 1997, 55, R4015-R4018.
22. S. Scheel, L. Knoll, D. G. Welsch and S. M. Barnett, *Phys Rev A*, 1999, 60, 1590-1597.
23. M. S. Tomas and Z. Lenac, *Phys Rev A*, 1997, 56, 4197-4206.
24. M. S. Tomas and Z. Lenac, *Phys Rev A*, 1999, 60, 2431-2437.
25. G. C. des Francs, C. Girard, J. C. Weeber, C. Chicane, T. David, A. Dereux and D. Peyrade, *Phys Rev Lett*, 2001, 86, 4950-4953.
26. C. Sauvan, J. P. Hugonin, I. S. Maksymov and P. Lalanne, *Phys Rev Lett*, 2013, 110.
27. C. Van Vlack and S. Hughes, *Opt Lett*, 2012, 37, 2880-2882.
28. N. Engheta, A. Salandrino and A. Alu, *Phys Rev Lett*, 2005, 95.
29. N. Engheta, *Science*, 2007, 317, 1698-1702.
30. A. Partovi, D. Peale, M. Wuttig, C. A. Murray, G. Zydzik, L. Hopkins, K. Baldwin, W. S. Hobson, J. Wynn, J. Lopata, L. Dhar, R. Chichester and J. H.-J. Yeh, *Applied Physics Letters*, 1999, 75, 1515-1517.
31. F. Chen, A. Itagi, J. Bain, D. Stancil, T. Schlesinger, L. Stebounova, G. Walker and B. Akhremitchev, *Applied Physics Letters*, 2003, 83, 3245-3247.
32. B. Guo, G. Song and L. Chen, *Journal of Optics A: Pure and Applied Optics*, 2008, 10, 085202.
33. H. Gai, J. Wang, Q. Tian, W. Xia and X. Xu, *Journal of Optics A: Pure and Applied Optics*, 2007, 9, 998.
34. J.-x. Gao, G.-f. Song, Q.-q. Gan, B. Guo and L. Chen, *Laser Physics Letters*, 2007, 4, 234-237.
35. B. Guo, G. Song and L. Chen, *Applied Physics Letters*, 2007, 91, 021103-021103-021103.
36. Z. Rao, L. Hesselink and J. S. Harris, *Opt Express*, 2007, 15, 10427-10438.

37. N. Yu, J. Fan, Q. J. Wang, C. Pflügl, L. Diehl, T. Edamura, M. Yamanishi, H. Kan and F. Capasso, *Nature Photonics*, 2008, 2, 564-570.
38. N. Yu, R. Blanchard, J. Fan, F. Capasso, T. Edamura, M. Yamanishi and H. Kan, *Applied Physics Letters*, 2008, 93, 181101.
39. J. Tetienne, R. Blanchard, N. Yu, P. Genevet, M. Kats, J. Fan, T. Edamura, S. Furuta, M. Yamanishi and F. Capasso, *New Journal of Physics*, 2011, 13, 053057.
40. N. Yu, M. Kats, C. Pflügl, M. Geiser, Q. J. Wang, M. A. Belkin, F. Capasso, M. Fischer, A. Wittmann and J. Faist, *Applied Physics Letters*, 2009, 95, 161108-161103.
41. R. Blanchard, T. S. Mansuripur, B. Gokden, N. Yu, M. Kats, P. Genevet, K. Fujita, T. Edamura, M. Yamanishi and F. Capasso, *Applied Physics Letters*, 2013, 102, 191114-191114-191115.
42. Y. Nanfang, W. Qi Jie, C. Pflügl, L. Diehl, F. Capasso, T. Edamura, S. Furuta, M. Yamanishi and H. Kan, *Applied Physics Letters*, 2009, 94, 151101-151101-151103.
43. N. Yu, Q. J. Wang, M. A. Kats, J. A. Fan, S. P. Khanna, L. Li, A. G. Davies, E. H. Linfield and F. Capasso, *Nat. Mater.*, 2010, 9, 730-735.
44. G. Liang, H. Liang, Y. Zhang, S. P. Khanna, L. Li, A. Giles Davies, E. Linfield, D. Fatt Lim, C. Seng Tan and S. Fung Yu, *Applied Physics Letters*, 2013, 102, 031119-031119-031114.
45. E. Cubukcu, E. A. Kort, K. B. Crozier and F. Capasso, *Applied Physics Letters*, 2006, 89, -.
46. X. Shi and L. Hesselink, *Japanese journal of applied physics*, 2002, 41, 1632.
47. N. Yu, E. Cubukcu, L. Diehl, M. A. Belkin, K. B. Crozier, F. Capasso, D. Bour, S. Corzine and G. Hofler, *Applied Physics Letters*, 2007, 91, 173113-173113-173113.
48. D. Dey, J. Kohoutek, R. M. Gelfand, A. Bonakdar and H. Mohseni, *Opt Lett*, 2010, 35, 2783-2785.
49. D. Dey, J. Kohoutek, R. M. Gelfand, A. Bonakdar and H. Mohseni, *Photonics Technology Letters, IEEE*, 2010, 22, 1580-1582.
50. D. Austin, N. Mullin, I. Luxmoore, I. Sandall, A. Cullis, A. Bismuto, J. Faist, J. Hobbs and L. Wilson, *Applied Physics Letters*, 2010, 96, 151105-151105-151103.
51. D. Austin, N. Mullin, A. Bismuto, I. Luxmoore, A. Adawi, D. Revin, M. Soulby, J. Cockburn, Q. Jiang and A. Krysa, *Photonics Technology Letters, IEEE*, 2010, 22, 1217-1219.
52. N. Yu, E. Cubukcu, L. Diehl, D. Bour, S. Corzine, J. Zhu, G. Höfler, K. B. Crozier and F. Capasso, *Opt. Express*, 2007, 15, 13272-13281.
53. R. M. Gelfand, D. Dey, J. Kohoutek, A. Bonakdar, S. C. Hur, D. D. Carlo and H. Mohseni, *Optics and Photonics News*, 2011, 22, 32-37.
54. J. Kohoutek, D. Dey, A. Bonakdar, R. Gelfand, V. Fathipour, O. G. Memis and H. Mohseni, *Small*, 2012, 8, 3781-3785.
55. Q. Qin, B. S. Williams, S. Kumar, J. L. Reno and Q. Hu, *Nature Photonics*, 2009, 3, 732-737.
56. J. Kohoutek, A. Bonakdar, R. Gelfand, D. Dey, I. Hassani Nia, V. Fathipour, O. G. Memis and H. Mohseni, *Nano letters*, 2012, 12, 2537-2541.
57. P. Dawson, D. Walmsley, H. Quinn and A. Ferguson, *Phys Rev B*, 1984, 30, 3164.
58. K. Okamoto, I. Niki, A. Shvartser, Y. Narukawa, T. Mukai and A. Scherer, *Nat. Mater.*, 2004, 3, 601-605.
59. A. Kock, E. Gornik, M. Hauser and W. Beinstingl, *Applied Physics Letters*, 1990, 57, 2327-2329.
60. J. Vuckovic, M. Loncar and A. Scherer, *Quantum Electronics, IEEE Journal of*, 2000, 36, 1131-1144.
61. D. Arbel, N. Berkovitch, A. Nevet, A. Peer, S. Cohen, D. Ritter and M. Orenstein, *Opt Express*, 2011, 19, 9807-9813.
62. S. Mokkaapati, D. Saxena, H. H. Tan and C. Jagadish, *Small*, 2013, 9, 3964-3969.
63. C.-Y. Cho, Y. Zhang, E. Cicek, B. Rahnema, Y. Bai, R. McClintock and M. Razeghia, *Applied Physics Letters*, 2013, 102, 211110.
64. A. Boltasseva and H. A. Atwater, *Science*, 2011, 331, 290-291.
65. A. Dentai, R. Kuchibhotla, J. Campbell, C. Tsai and C. Lei, *Electronics Letters*, 1991, 27, 2125-2127.
66. K. Kishino, M. S. Unlu, J.-I. Chyi, J. Reed, L. Arsenault and H. Morkoc, *Quantum Electronics, IEEE Journal of*, 1991, 27, 2025-2034.
67. A. Rogalski, *Prog. Quantum Electron.*, 2003, 27, 59-210.
68. V. Lopes, A. Syllaios and M. Chen, *Semiconductor Science and Technology*, 1993, 8, 824.
69. A. Rogalski, *J Appl Phys*, 2003, 93, 4355-4391.
70. K. C. Balram, R. M. Audet and D. A. Miller, *Opt Express*, 2013, 21, 10228-10233.
71. P. Fan, K. C. Huang, L. Cao and M. L. Brongersma, *Nano letters*, 2013, 13, 392-396.
72. F.-F. Ren, K.-W. Ang, J. Ye, M. Yu, G.-Q. Lo and D.-L. Kwong, *Nano letters*, 2011, 11, 1289-1293.
73. T. J. Seok, A. Jamshidi, M. Eggleston and M. C. Wu, *Opt Express*, 2013, 21, 16561-16569.
74. K. C. Balram and D. A. Miller, *Opt. Express* 20 (20), 2012, 22735-22742.
75. J. K. Hyun and L. J. Lauhon, *Nano letters*, 2011, 11, 2731-2734.
76. L. Cao, J.-S. Park, P. Fan, B. Clemens and M. L. Brongersma, *Nano letters*, 2010, 10, 1229-1233.
77. S. Collin, F. Pardo, N. Bardou, A. Lemaître, S. Averin and J.-L. Pelouard, *Opt Express*, 2011, 19, 17293-17297.
78. S. Kalchmair, R. Gansch, S. Ahn, A. Andrews, H. Detz, T. Zederbauer, E. Mujagić, P. Reininger, G. Lasser and W. Schrenk, *Opt Express*, 2012, 20, 5622-5628.
79. R. V. Shenoi, J. Rosenberg, T. E. Vandervelde, O. J. Painter and S. Krishna, *Quantum Electronics, IEEE Journal of*, 2010, 46, 1051-1057.
80. S. Lee, S. Krishna and S. Brueck, *Photonics Technology Letters, IEEE*, 2011, 23, 935-937.
81. Y. Nga Chen, Y. Todorov, B. Askenazi, A. Vasanelli, G. Biasiol, R. Colombelli and C. Sirtori, *Applied Physics Letters*, 2014, 104, -.
82. X. W. Chen, M. Agio and V. Sandoghdar, *Phys Rev Lett*, 2012, 108.
83. H. Walther, B. T. H. Varcoe, B. G. Englert and T. Becker, *Rep Prog Phys*, 2006, 69, 1325-1382.
84. D. Brinks, M. Castro-Lopez, R. Hildner and N. F. van Hulst, *Proceedings of the National Academy of Sciences of the United States of America*, 2013, 110, 18386-18390.
85. T. Schumacher, K. Kratzer, D. Molnar, M. Hentschel, H. Giessen and M. Lippitz, *Nat Commun*, 2011, 2.
86. W. Bao, M. Melli, N. Caselli, F. Riboli, D. S. Wiersma, M. Staffaroni, H. Choo, D. F. Ogletree, S. Aloni, J. Bokor, S. Cabrini, F. Intonti, M. B. Salmeron, E. Yablonovitch, P. J. Schuck and A. Weber-Bargioni, *Science*, 2012, 338, 1317-1321.
87. J. N. Chen, M. Badioli, P. Alonso-Gonzalez, S. Thongrattanasiri, F. Huth, J. Osmond, M. Spasenovic, A. Centeno, A. Pesquera, P. Godignon, A. Z. Elorza, N. Camara, F. J. G. de Abajo, R. Hillenbrand and F. H. L. Koppens, *Nature*, 2012, 487, 77-81.
88. Y. Yao, M. A. Kats, P. Genevet, N. F. Yu, Y. Song, J. Kong and F. Capasso, *Nano Letters*, 2013, 13, 1257-1264.
89. X. M. W. L. Shao, H. T. Xu, J. F. Wang, J.-B. Xu, L.-M. Peng, H.-Q. Lin, *Adv Opt Mater*, 2014, 2, 162-170.